upon ν and the initial conditions applied at $\nu = \nu_0$. In any practical situation, this must be a real-time operation.

References

[1] Zlatoustov, U. A. et al., "Investigation of Satellite Oscillations in the Plane of an Elliptic Orbit," *Proceedings of the 11th International Congress of Applied Mechanics*, Springer-Verlag, Berlin, 1966, pp. 436–439.

[2] Brereton, R. C. and Modi, V. J., "On the Stability of Planar Librations of a Dumbbell Satellite in an Elliptic Orbit," *Journal of the Royal Aeronautical Society*, Vol. 70, No. 672, Dec. 1966, pp. 1098–1102.

[3] Graham, D. and McRuer, D., *Analysis of Nonlinear Control Systems*, Wiley, New York, 1961, p. 70.

[4] Frick, R. H. and Garber, T. B., "General Equations of a Motion of a Satellite in a Gravitational Gradient Field," Rept. RM-2527, Dec. 1959, The Rand Corp.

[5] Baker, R. M. L., "Librations on a Slightly Eccentric Orbit," *ARS Journal*, Vol. 30, No. 1, Jan. 1960, pp. 124–126.

[6] Whisnant, J. M. and Anand, D. K., "Roll Resonance for a Gravity-Gradient Satellite," *Journal of Spacecraft and Rockets*, Vol. 5, No. 6, June 1968, pp. 743–744.

[7] Whisnant, J. M. et al., "The Dynamic Modeling of Hysteresis and Application to Damping of Spacecraft Librations," AIAA Paper 69-833, Princeton, N.J., 1969.

[8] Anand, D. K., Whisnant, J. M., and Sturmanis, M., "The Capture and Stability of a Gravity-Gradient Satellite in an Eccentric Orbit," Rept. TG-1028, Aug. 1968, Applied Physics Lab., The Johns Hopkins Univ., Silver Spring, Md.

[9] Anand, D. K., Yuhasz, R. S., and Whisnant, J. M., "Further Comments on Attitude Motion in an Eccentric Orbit," TM, Applied Physics Lab., The Johns Hopkins Univ., Silver Spring, Md., in preparation.

Prediction of Flight Performance of a Throttling, Ablative Rocket Engine

ROBERT D. BAKER*

Systems Group of TRW Inc., Redondo Beach, Calif.

Nomenclature

A = cross-sectional area, in.^{2}
C,D,E = empirical constants
C_f = nozzle thrust coefficient, dimensionless
C^* = characteristic velocity, fps
F = engine vacuum thrust, lbf
g = mass equivalence = 32.174 lbm/slug
I_{sp} = engine specific impulse, lbf-sec/lbm
K = hydraulic conductance
L^* = chamber characteristic length, ft
M = mass of spacecraft, slugs
P = pressure, psia
ΔP = injector pressure drop, psid
r = radial distance, ft
Rm = mixture ratio, dimensionless
S = throttle position, percent of maximum
T = temperature, °R
t = measured burn time, sec
T_{120} = time required to erode a fiberglass nozzle throat 20%, sec
ΔV = characteristic velocity, fps
$\dot{w}$ = propellant flowrate, lbm/sec
α = injector momentum ratio, oxidizer/fuel
β = ratio of nozzle stagnation pressure to chamber pressure, dimensionless
θ = angular displacement, radians
λ = combustion chamber gas velocity function
μ = gravitation constant, ft^3/sec^2
ρ = fluid density, lbm/ft^3
τ = time dummy variable, sec
ϕ = thrust vector angle from local horizontal, deg
Ψ = error function, dimensionless

Subscripts

t = nozzle throat, total
o = original or initial, oxidizer
i = vector index, interface, station in flow system
c = chamber
e = engine, combustion gas
f = fuel
n = nozzle

Presented as Paper 69-452 at the AIAA 5th Propulsion Joint Specialist Conference, U.S. Air Force Academy, Colo., June 9–13, 1969; submitted June 4, 1969; revision received September 2 ,1969.

* Head, Flight Systems Section, Professional Engineer, Senior Lecturer in Engineering, University of Southern Calif. Member AIAA.

Introduction

IN simulating the performance of a throttling, ablative rocket engine system, variations of performance with respect to the engine throttle position must be considered in addition to performance deviations produced by off-nominal engine interface conditions and throat erosion. Performance parameters such as vehicle ΔV gain, delivered impulse, and propellant consumption are dependent upon the throttle time profile employed during the mission as well as the initial performance measured during acceptance tests of the engine. If the engine is to be used on a soft-landing mission, it will be necessary to augment the engine performance characterization with the actual dynamic constraints of the flight path. Such a capability has been developed at TRW Systems to simulate the performance of the lunar module descent engine (LMDE) executing a lunar landing mission (LLM).

Discussion

Analysis can be carried out assuming a fixed throttle-time profile representing a nominal mission or the model can be augmented with the actual dynamic equations describing the accelerations experienced while transiting a conservative centralized inverse square force field. Usual simplifying assumptions for an LLM are: spherical moon without gravitational perturbations, two-dimensional flight in the equatorial plane, and no drag. The equations of motion for this problem in polar coordinates are

$$r\ddot{\theta} + (F/M)\cos\phi + 2\dot{r}\dot{\theta} = 0 \quad (1)$$

$$\ddot{r} - r\dot{\theta}^2 + (F/M)\sin\phi + \mu/r^2 = 0 \quad (2)$$

Figure 1 illustrates the directions of these acceleration terms. The targeted speed and altitude parameters then act as the constraints for the mission. To meet these constraints in the nominal case the LMDE throttle-time profile is as shown in Fig. 2. The remainder of the propulsion system simulation model can be constructed in either one of two ways, by use of an influence coefficient model or a nonlinear model.

Influence Coefficient Method

The most compact and simplest form is to take a linear approach wherein the basic external performance parameters (P_c,Rm,F,$\dot{w}_t$, and hence I_{sp}) are tabulated against throttle position for nominal engine operation. Critical performance parameters are then determined in the nominal case by interpolating the table based on the required throttle position. Off-nominal conditions are accounted for by the use of linear influence factors on the tabulated parameters. Off-nominal conditions† are considered to be produced by external factors.

The accelerations required to meet the speed and altitude constraints shown in Fig. 1 are augmented with the instantaneous mass of the vehicle and the required throttle position

† Such as off-nominal interface pressure, temperatures, gas absorption within propellants, etc.

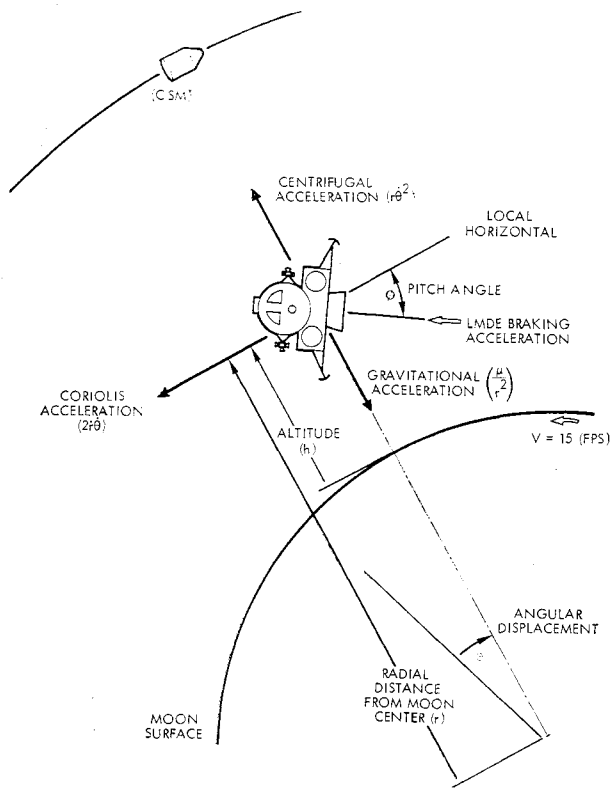

Fig. 1 Two-dimensional acceleration relationships as used by Victory VIII in simulation of a lunar module descent flight.

and pitch angle are thus determined. The performance at that particular throttle position is interpolated from the nominal performance table. The instantaneous throat area is determined by integrating up to that point in time a throat erosion rate characterization model. Therefore, at each instant in time the parameters are adjusted, as shown in Eq. (3), for throat area and feed system variations by the application of the indicated influence coefficients‡;

$$\begin{vmatrix} F_2 \\ I_{sp_2} \\ Rm_2 \\ \alpha_2 \end{vmatrix} = \begin{vmatrix} F_o \\ I_{sp_o} \\ Rm_o \\ \alpha_o \end{vmatrix} + \begin{vmatrix} \frac{\partial F}{\partial A_t} \\ \frac{\partial I_{sp}}{\partial A_t} \\ \frac{\partial Rm}{\partial A_t} \\ \frac{\partial \alpha}{\partial A_t} \end{vmatrix} \cdot \{\Delta A_t\} + \begin{vmatrix} \frac{\partial F}{\partial P_{eio}} & \frac{\partial F}{\partial P_{eif}} & \frac{\partial F}{\partial T_o} & \frac{\partial F}{\partial T_f} \\ \frac{\partial I_{sp}}{\partial P_{eio}} & \frac{\partial I_{sp}}{\partial P_{eif}} & \frac{\partial I_{sp}}{\partial T_o} & \frac{\partial I_{sp}}{\partial T_f} \\ \frac{\partial Rm}{\partial P_{eio}} & \frac{\partial Rm}{\partial P_{eif}} & \frac{\partial Rm}{\partial T_o} & \frac{\partial Rm}{\partial T_f} \\ \frac{\partial \alpha}{\partial P_{eio}} & \frac{\partial \alpha}{\partial P_{eif}} & \frac{\partial \alpha}{\partial T_o} & \frac{\partial \alpha}{\partial T_f} \end{vmatrix} \cdot \begin{Bmatrix} \Delta P_{eio} \\ \Delta P_{eif} \\ \Delta T_o \\ \Delta T_f \end{Bmatrix} \quad (3)$$

Nonlinear Propulsion Model

A second and more involved method of engine model construction involves a nonlinear approach wherein the hydraulic conductances are first characterized for the engine system. Figure 3 illustrates the conductances as utilized for the LMDE. The hydraulic conductance for any subcomponent of the feed system is defined as

$$K_{1-2} = \dot{w}/[(P_1 - P_2)\rho]^{1/2} \quad (4)$$

Formally, this definition of conductance is equal to the product of the discharge coefficient and the flow area. It assumes an incompressible inviscid fluid, undergoing streamline flow, with no change in potential energy. Furthermore, the upstream and downstream velocities are considered equal with steady-state conditions prevailing.

These conductances are computed, usually during an engine's acceptance test series, to form the basis of the hydraulic characterization. The hydraulic conductances are then combined with the interface pressures to compute the flow rate through the oxidizer and fuel passes using Eq. (4). The back pressure on the system, of course, is the head end chamber pressure which directly relates to the combustion chamber characteristic velocity C^*, and the ratio of nozzle stagnation to head end chamber pressure β. Throttling is simulated by making the variable conductances a function of the throttle position, providing that flow upstream of the combustion chamber is not critical (i.e., cavitating). However, in the case of the LMDE, critical flow control valve operation is utilized upstream of the combustion chamber for the purpose of throttling and maintaining propellant flow rates independent of chamber pressure. This being the case, the critical conductances become the controlling conductances and are computed by replacing in Eq. (4) the P_2 with the vapor pressure of the fluid. The vapor pressure is a function of temperature. Furthermore, this cavitating conductance is the exclusive controlling conductance for the flow through any subsequent tandem stations. This effect resembles choked nozzle flow. Providing the temperature of the flowing medium remains constant, the flow would be essentially regulated by the critical conductance which relates to the passage geometry and the inlet pressure and would be independent of any downstream or back pressure. However, should there not be a critical operation upstream of the combustion chamber, then P_c becomes the back (or discharge) pressure of the hydraulic system, thus requiring a recursive solution to balance the engine hydraulic model.

The most successful model for C^* in the case of the LMDE, has been developed around the C^* efficiency parameter $\eta_c{}^*$;

$$\eta_c{}^* = E_1 + E_2\Delta P_o + E_3\Delta P_f + E_4\Delta P_o{}^2 + E_5\Delta P_f{}^2 + E_6\Delta P_o\Delta P_f + E_7\Delta A_t \quad (5)$$

$$C^*_{th} = f(P_{nt}, Rm) \quad (6)$$

The back pressure is then

$$P_c = C^*\dot{w}_t/\beta A_t g \quad (7)$$

The internal performance evaluation,§ directly leads us to the LMDE model for the thrust coefficient C_f as given later.

One of the advantages of this method over the influence coefficient method, other than the obvious increase in accuracy, is that uncertainties in all the particular component conductances as well as in the performance characterization models can be included, and an effective sensitivity analysis can be conducted to determine the over-all uncertainty of any particular prediction. As in the case of the influence coefficient model, the throat erosion rate function is integrated over the engine flight profile.

Throat Erosion

The throat erosion rate varies: 1) from one piece of hardware to another and must be tied to an acceptance test ob-

‡ These influence coefficients can also be a function of throttle position.

§ Characterization of $C^*(L^*)$ is included in the term ΔA_t of Eq. (5).

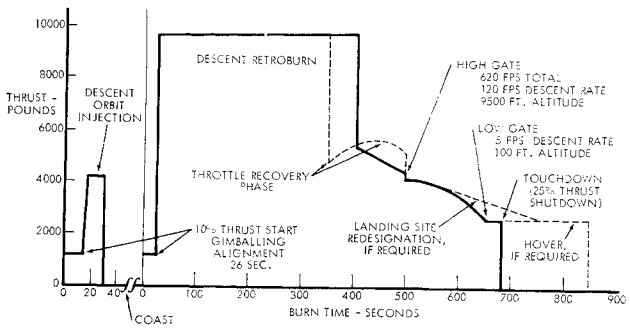

Fig. 2 Preliminary mission "G" lunar landing.

servation, 2) directly with chamber pressure, 3) inversely with accumulated erosion, 4) directly with the local mixture ratio near the walls, and 5) directly with total mixture ratio¶ (combustion gas temperature).

The throat erosion rate model used successfully in the LMDE characterization is as follows:

$$dA_t/dt + G(S)A_t + H[f(T_{120}),S,\alpha,F,\tau] = 0 \quad (8)$$

where

$$G(S) = -D_3\left\{D_6 + D_7 \tan^{-1}\left(\sum_{i=8}^{10} D_i S^{(i-8)}\right)\right\} \quad (9)$$

$$H[f(T_{120}),S,\alpha,F,\tau,] = -[(D_1/T_{120})^{D_2} + D_4(S - \bar{S}) + D_5(\alpha - \bar{\alpha})]\cdot G(S) - B(F,t) \pm n\dot{\sigma} \quad (10)$$

$$B(F,t) = D_{11}\exp\left(-D_{12}\int_0^t F d\tau\right) \quad (11)$$

$$f(T_{120}) = \begin{cases} T_{120} \text{ at } FTP \text{ for } S > 73\% \\ 80 \text{ for } S \leq 73\% \end{cases} \quad (12)$$

This throat erosion rate model is essentially a first-order Taylor series expansion of the variables throat area (A_t), throttle position (S) (actually representing chamber pressure), injector momentum ratio (α), an indication of the local mixture ratio at the wall, and time (t). The erosion rate model is biased by $f(T_{120})$ for each individual engine unit based on ablative testing of that particular unit utilizing a Fiberglas chamber and throat. This is the time required for a standardized Fiberglas throat to erode 20% in throat area. Relationships have been developed to correlate the erosion rate experienced on the Fiberglas throat with that encountered when the silica flight hardware is utilized.

Silica based chambers and throats characteristically display a glassing or swelling effect during the first portions of any burn (see Fig. 4). This is predominately due to the influx of moulten silica from the surface layers of the ablative material into the gas stream and onto the chamber walls. To the gas flow in the combustion chamber this appears as a constriction in the throat area. With LMDE, this phenomenon prevails for approximately 100 to 200 sec, depending on the throttle position, before the silica within the surface layers is sufficiently driven off such that erosion of the "dried-out" surface material can now take place. The term $B(F,t)$, Eq. (11), is a function which accounts for this initial swelling effect. It can be seen that the term exponentially decays with accumulated impulse; i.e., initial burns at higher throttle positions would tend to dry out the surface material of the chamber faster.

The multiplier function $G(S)$, Eq. (9), insures that the predicted erosion rate becomes independent of parameters such as T_{120}, A_t, and injector momentum ratio α, at very low throttle positions. The over-all uncertainty for the equation is expressed as an erosion rate ($\dot{\sigma}$); hence, when integrated, the amount of predicted erosion uncertainty will directly increase with time.

¶ Assuming hypostoichiometric mixture ratio, otherwise the converse.

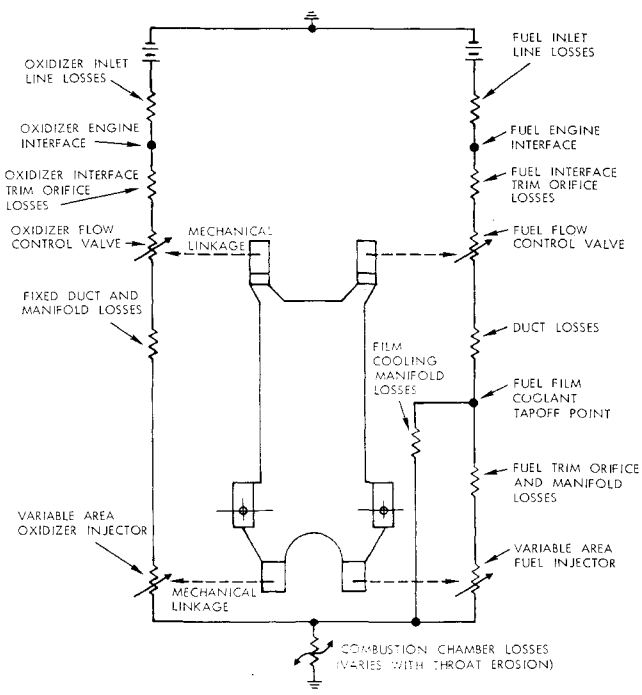

Fig. 3 Analogous electrical schematic of LMDE propellant flow system.

Method for Evaluating $A_t(t)$

The most successful method found thus far utilizes a variational approach by determining coefficients to three linearized internal performance parameter models. The internal performance parameters are expressed by linear expansions with undetermined coefficients. The throat area is expressed as an orthogonal polynomial series expansion of burn time. An error function is then formed and optimized with respect to the undetermined coefficients. After the analyses of several units of a particular engine system the numerical values of the internal performance parameter model coefficients should become stabilized. This method is advantageous in that it simultaneously develops performance models for the engine system while reducing the static test data. To effect this scheme, one should proceed as follows. From the definitions of C^*, β, and C_f we obtain

$$P_c\beta A_t C_f/F = 1 \quad (13)$$

The performance parameters not directly measured are then functionally expressed as

$$A_t = \sum_{i=1}^{m} C_i t^{(i-1)} \ (m = 7) \quad (14)$$

$$\beta = \beta_0 + \partial\beta/\partial\lambda(\lambda - \lambda_0) + \partial\beta/\partial A_t(A_t - A_{t0}) \quad (15)$$

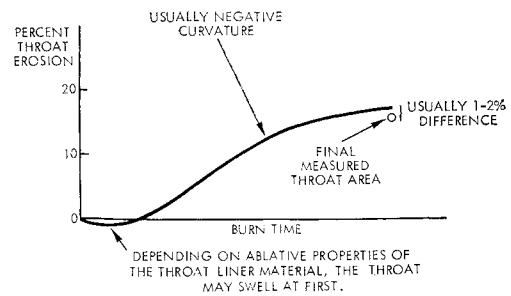

Fig. 4 Typical variation of throat area with burn time.

where

$$\lambda = \dot{w}_t T_e / P_c = f \text{ (axial chamber gas velocity)} \quad (16)$$

$$C_f = C_{fo} + \partial C_f/\partial P_{nt}(P_{nt} - P_{nto}) + \partial C_f/\partial Rm(Rm - Rm_o) + \partial C_f/\partial A_t(A_t - A_{to}) \quad (17)$$

Fourteen variables [assuming Eq. (14) has seven terms] are involved. These are: C_1–C_7 in Eq. (14); $C_8 = \beta_o$, $C_9 = \partial\beta/\partial\lambda$, and $C_{10} = \partial\beta/\partial A_t$ in Eq. (15); and $C_{11} = C_{fo}$, $C_{12} = \partial C_f/\partial P_{nt}$, $C_{13} = \partial C_f/\partial Rm$, and $C_{14} = \partial C_f/\partial A_t$ in Eq. (17).

Values for β_o and C_{fo} (at the rated point, no erosion) are chosen to correspond to values of λ_o, A_{to}, P_{nto}, and Rm_o. It is recommended that these relationships be established in the following order: A_{to} = noneroded throat area; λ_o = chamber velocity function evaluated at the full thrust position with A_{to}; $\beta_o = P_{nto}/P_o$ at λ_o and A_{to}; and C_{fo} = thrust coefficient at P_{nto}, A_{to}, and Rm_o. It is then assumed that all of the undetermined partial derivatives are constants. Equation (13) is rearranged, squared, and summed over the entire test duration (i.e., data slice, by slice) to obtain the error function Ψ;

$$\Psi = \frac{1}{N}\sum_{i=1}^{N}\left(\frac{P_c}{F}\beta A_t C_f - 1\right)_i^2 \quad (18)$$

where N = number of data slices.

The problem of minimizing Eq. (18) readily lends itself to a digital computer solution. Initial values for C_1–C_7 are determined by assuming a C^* for each data slice during the test duration, then estimating A_t. Data from similar past tests are very useful at this point in order to initialize C_1–C_7 more accurately by a least-squares (usually 6th degree or larger) fit of the "first cut" $A_t(t)$ data. Coefficients C_8–C_{14} can be initialized from theoretical considerations, past test data, or engineering judgment. The most important aspect in initializing C_9–C_{14} is determining the correct order of magnitude and sign.

The task of minimizing Eq. (18) becomes that of setting all the first partial derivatives equal to zero. Initially the steepest rate of descent method was used with the first and second partial derivatives being computed numerically. The particular independent variable possessing the second partial derivative of highest absolute magnitude was perturbed in an effort to set its first partial derivative to zero. The remaining variables were held constant, i.e.,

$$\Delta C_i = (0 - \partial\Psi/\partial C_i)/(\partial^2\Psi/\partial C_i^2) \quad (19)$$

where Ψ = error function (18).

This process was repeated in a recursive manner until the numerical values of all of the first partial derivatives were approximately zero. This method proved cumbersome in that it completely ignored the off-diagonal terms of the second partial derivative matrix. Convergence was improved when these off-diagonal terms were taken into account. A second algorithm employed was only limited by the errors associated with the numerical calculation of the first and second partial derivatives;

$$[\Delta C_j] = [\partial^2\Psi/\partial C_{ij}^2]^{-1}\cdot[0 - \partial\Psi/\partial C_i], \quad i = 1, \ldots, 14; \quad j = 1, \ldots, 14 \quad (20)$$

It was impossible to set the first partial derivatives exactly to zero; however, values in the order of 0.001 (nondimensionalized) were obtained.

A breakthrough on this method was realized when more elaborate optimization algorithms were employed such as those contained in SLANG,** a TRW Systems engineering modeling language for system simulation and optimization. SLANG has the advantage that, as part of its compiler functions, it automatically programs the first and second partial derivatives from the original function (in this case, Ψ). This eliminated the errors inherent in numerical calculation of partial derivatives. Secondly, SLANG employs more elaborate optimization algorithms with various safeguards for purposes of maintaining the solution continuity and preventing "blow-ups." The time required to minimize Ψ was reduced by a factor of 10, and the magnitude of Ψ was reduced by a factor of 20, as compared to the former methods.

** SLANG™, copyright, 1968, TRW Inc., Redondo Beach, Calif.

Low-Thrust, Constant-Acceleration Trajectories for Solar Probe Missions

HARVEY T. BROCK JR.*
U.S. Air Force Academy, Colo.
AND
ROGER W. JOHNSON†
Air Force Institute of Technology, Wright-Patterson Air Force Base, Ohio

THE purpose of this investigation is to determine the feasibility of using tangential thrust, constant-acceleration trajectories for close solar probe missions. Trajectories to 0.05 a.u. using low-thrust electric engines are considered. Both HEV = 0 and HEV > 0 (hyperbolic excess velocities) after escape from the earth by chemical rocket are considered. Previous investigators of solar probe missions have considered constant-thrust trajectories with or without coast phases,[1-2] but, as far as we are able to determine, no reports on constant-acceleration trajectories for solar probe missions are in the open literature.

Several criteria are used to judge the usefulness of the various trajectories investigated. One of these is the total time T required for the probe to reach a point 0.05 a.u. from the sun. Current and projected electric-engine lifetimes are of the order of 10,000 hr (416 days).[3] An upper limit of 400 days is chosen for the time to reach the desired location. Another consideration is the total velocity change (decrease, ΔV) to be accomplished during the flight. The third criterion is the terminal angle ϕ between the sun-earth radius and the sun-probe radius. This angle should be 90° in order to have the best possible radio communication with the probe when it reaches 0.05 a.u. The initial assumptions are: 1) initially, boost to escape velocity is by a chemical

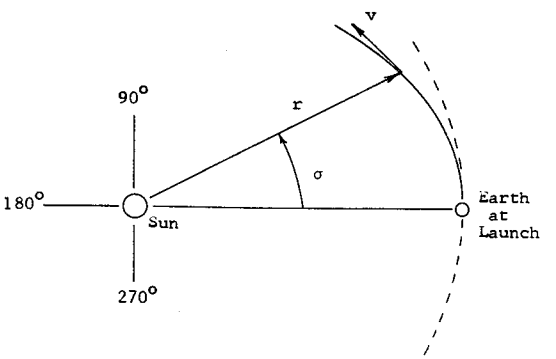

Fig. 1 Heliocentric-ecliptic coordinate system.

Received October 7, 1968; revision received September 12, 1969.

* Captain, U.S. Air Force, Instructor of Astronautics.

† Lt. Colonel, U.S. Air Force, Associate Professor of Electrical Engineering.